

EARLY ONLINE RELEASE

This is a PDF of a manuscript that has been peer-reviewed and accepted for publication. As the article has not yet been formatted, copy edited or proofread, the final published version may be different from the early online release.

This pre-publication manuscript may be downloaded, distributed and used under the provisions of the Creative Commons Attribution 4.0 International (CC BY 4.0) license. It may be cited using the DOI below.

The DOI for this manuscript is

DOI:10.2151/jmsj.2022-039

J-STAGE Advance published date: June 21st, 2022

The final manuscript after publication will replace the preliminary version at the above DOI once it is available.

1 **Spatial Structure and Formation Mechanism of Local**
2 **Winds “Suzuka-oroshi” at the Foothills of Suzuka**
3 **Mountains, Japan**

4
5 **Shunsuke YAMADA**

6 *Graduate School of Life and Environmental Sciences,*

7 *University of Tsukuba, Japan*

8 **and**

9 **Hiroyuki KUSAKA ¹**

10 *Center for Computational Sciences,*

11 *University of Tsukuba, Japan*

12
13 June 16, 2021

14
15
16 -----
17 1) Corresponding author: Hiroyuki Kusaka, Center for Computational Sciences, University
18 of Tsukuba

19 Email: kusaka@ccs.tsukuba.ac.jp

20 Tel: +81-29-853-6481

Abstract

We examined the essential features and formation mechanism of the strong local “Suzuka-oroshi” winds, which are located leeward of the Suzuka Mountains in Japan. This area features a favorable topography for downslope windstorms. Climatological analysis revealed that Suzuka-oroshi mainly occurred after an extratropical cyclone with a cold front and passed the Sea of Japan (55% of all occurrences). Additionally, inversion layers (1–5 km level) were observed in 74% of cases. Climatological analysis using spatially dense observational data showed that the strongest winds tended to blow in the northern part of the plain on the leeward side. Numerical simulations for one case by the Weather Research and Forecasting (WRF) model with 1 km grid increment supported this finding. Simulation results with and without the Suzuka Mountains demonstrated that the strong Suzuka-oroshi in the northern part of the plain comprised downslope windstorms with transition of flow regime (internal Froude number was less than 1.0 at the windward of mountains and larger than 1.0 above the leeward slope). Additionally, differences in height of the mountains between the north and south parts results in the greater wind speed in the northern parts compared to the southern parts.

Keywords: Suzuka-oroshi, local wind, downslope windstorm, local hydraulic theory, mountain wave

41 **1 Introduction**

42 Downslope windstorms are strong local winds that blow on the leeward slopes and
43 foothills of mountains, formed by the acceleration of air as they cross the mountains. These
44 winds occur in many places worldwide, including Foehn in the Alps (Gohm and Mayr 2004;
45 Zangl et al. 2004; Armi and Mayr 2007), Bora on the Adriatic coast (Yoshino, 1976; Smith
46 1985, 1987; Gohm and Mayr 2005), Chinook in the Rocky Mountains (Glenn 1961; Lilly and
47 Zipser 1972), and Antarctic Peninsula foehns (Orr et al., 2008; Elvidge et al., 2016, 2020;
48 Turton et al., 2018).

49 Theories to explain the occurrence of downslope windstorms were proposed in the
50 1980s and can be broadly summarized into two or three main theories (Durrán 1990;
51 Jackson et al 2003, Lin 2007). First is the local hydraulic theory (e.g., Smith 1985; Durrán
52 1986) that extends classical shallow water theory (Houghton and Kasahara 1968; Arakawa
53 1968, 1969) to the atmosphere with stratification. In this theory, flow in the lower layers of
54 the well-mixed region such as wave-breaking region behaves locally as a shooting
55 (supercritical) flow. Specifically, flows approaching the mountains are divided by the well-
56 mixed region above the mountains and accelerate below this region. Second is the resonant
57 amplification theory that was proposed in a series of studies performed by Peltier and Clark
58 (Peltier and Clark 1979, 1983; Clark and Peltier, 1984). They described that the severe
59 downslope windstorms occur due to nonlinear resonance between upward and downward
60 mountain waves reflected at the critical layer. The third is the vertical energy transport theory

61 that is linear theory (Klemp and Lilly 1975). Durran and Klemp (1987) examined the critical
62 level height for stage of severe downslope windstorms state, the results of which supported
63 Smith's theory. Currently, it is considered that Peltier-Clark's and Smith's theories explain
64 flows at the earlier and mature stages of severe downslope windstorm development,
65 respectively (Lin 2007).

66 Downslope windstorms easily occur in straight mountain ranges and in terrains where
67 the leeward slope is steeper than the windward slope (Raymond 1972; Lilly and Klemp 1979;
68 Pitts and Lyons 1989; Miller and Durran 1991; Saito and Ikawa 1991). Furthermore,
69 downslope windstorms easily occur over mountains with saddles because hydraulic jumps
70 are less likely to occur leeward of saddles and strong wind regions extend farther leeward
71 (Raymond 1972; Lilly and Klemp 1979; Pitts and Lyons 1989; Miller and Durran 1991; Saito
72 1993; Gohm et al. 2008; Elvidge and Renfew 2016).

73 The conditions favored by downslope windstorms are affected by the terrain shape and
74 atmospheric condition. The mountain Froude number Fr (or its inverse, the non-dimensional
75 mountain height) is often used as an indicator of the occurrence of downslope windstorms
76 and/or mountain-wave breaking. Lin and Wang (1996) investigated the relationship between
77 Fr and the behavior of airflows over mountains using a two-dimensional idealized model (Eq.
78 (1)).

$$79 \quad Fr = U/NH \quad (1)$$

80 Here, U is the wind speed of the approaching flow, N is the Brunt-Väisälä frequency, and H

81 is the mountain height. Lin and Wang (1996) found that downslope windstorms occur when
82 Fr is approximately 0.6–1.2, and other studies showed similar results (Gabersek and Durran
83 2004). The presence of a temperature inversion layer and critical layer facilitates the
84 formation of downslope windstorms (Klemp and Durran 1987; Smith and Skillingstad 2011).
85 The role of the inversion layer in downslope windstorm occurrences can be approximately
86 divided into the following two categories. In the presence of an inversion layer at a lower
87 level, airflow over the mountains easily transitions from subcritical flow to supercritical flow,
88 facilitating the occurrence of downslope windstorms. The presence of an inversion layer at
89 the upper level also makes it easier to induce mountain-wave breaking just below this layer
90 because of the reflection and resonance of mountain waves, in turn making it easier for
91 downslope windstorms to blow under the well mixed region.

92 Downslope windstorms are common in Japan because of the complex and undulating
93 topographies of the country's islands, which are unique to each region. Japan's well-known
94 downslope windstorms include the "Yamaji-kaze" (Saito and Ikawa 1991; Saito 1993, 1994),
95 "Hiroto-kaze" (Fudeyasu et al. 2008), "Karakkaze" (Yoshino 1975, 1986; Kusaka et al. 2011;
96 Nishi and Kusaka 2019a, b), "Inami-kaze" (Koyanagi and Kusaka 2020), "Jintsu-oroshi"
97 (Kusaka et al. 2021), "Zao-oroshi" (Sawada et al. 2012), "Chokai-oroshi" (Asano and Kusaka
98 2022), and "Suzuka-oroshi" (Owada, 1990; Komatsu and Tachibana, 2016). The "Kiyokawa-
99 dashi" is thought to be gap winds but exhibits characteristics of downslope windstorms
100 (Yoshino 1986; Ishii et al. 2007; Sasaki et al. 2005, 2010). Japan's local winds, including

101 downslope windstorms, have been summarized by Yoshino (1986) and Kusaka and
102 Fudeyasu (2017).

103 A strong westerly wind known as "Suzuka-oroshi" blows in the eastern plains at the
104 base of the Suzuka Mountains (Yoshino 1975). The Suzuka Mountains are in the Mie and
105 Shiga prefectures and are north-south oriented (Fig. 1). These mountains are divided into
106 three parts: the northern part comprises a series of mountains that are approximately 1,000
107 m in height, mountains in the central part are approximately 500 m, and those in the southern
108 part are approximately 800 m in height. The Suzuka Pass, a major transportation hub with
109 highways, is in the central part of the Suzuka Mountains. The Suzuka Mountains are highly
110 asymmetric range; the eastern slopes are steeper than the western slopes. Therefore, the
111 terrain of the Suzuka Mountains can make them prone to downslope windstorms.

112 Owada (1990) clarified the climatological characteristics of Suzuka-oroshi using
113 Automated Meteorological Data Acquisition System (AMeDAS) data for the area to the south
114 (i.e., leeward) of the Suzuka Mountains. He identified the Suzuka-oroshi as winds with
115 surface wind speeds of at least 8 m s⁻¹ and found that Suzuka-oroshi was more likely to
116 blow during the winter and spring, during the daytime, under a typical pressure pattern in
117 the winter (that is a pressure pattern with the Siberian High to the west of Japan, a low to
118 the east of Japan) (Fig. 2a, b). Analysis of the distribution of wind-shaped trees (wind-
119 deformed tree) showed that Suzuka-oroshi tend to blow in the central and southern part of
120 the plain where is located at the leeward the Suzuka Mountains. Komatsu and Tachibana

121 (2016) also reported that Suzuka-oroshi blow in the southern part of the plain, using the
122 AMeDAS surface wind data. Although Suzuka-oroshi have been studied, four open
123 questions remain at least.

124 The first question concerns the spatial distribution of Suzuka-oroshi. According to the
125 principal of the local elementary school and fire department officer living in the areas shown
126 in Fig. 1, the Suzuka-oroshi blow in the leeward area of the northern part of the Suzuka
127 Mountains. These local residents' perceptions are not consistent with the results of the
128 previous studies (Owada 1990; Komatsu and Tachibana 2016).

129 The second question concerns the favorable synoptic weather pattern during Suzuka-
130 oroshi events. Owada (1990) analyzed the synoptic weather pattern when the surface wind
131 speed was 8 m s⁻¹ or higher (Fig. 2a, b). However, according to our interviews, the local
132 people recognize Suzuka-oroshi as strong enough to cause large branches of trees to sway,
133 power lines to roar, and people to feel threatened. This is equivalent to a wind speed of 11
134 m s⁻¹ by the Beaufort Scale: "The large branches of the trees sway, making it difficult to hold
135 an umbrella. Power lines squeal " (strong breeze, wind speed 10.8–13.8 m s⁻¹ at 10 m
136 above ground). Therefore, Owada (1990) may not have captured the typical pressure
137 pattern that occurs when Suzuka-oroshi blows.

138 The third and fourth questions concern the favorable mesoscale atmospheric conditions
139 for Suzuka-oroshi and their formation mechanisms. The relationship between Suzuka-oroshi,
140 the inversion layer, and *Fr* remains unclear. Regarding the mechanism of Suzuka-oroshi,

141 Komatsu and Tachibana (2016) launched six sondes at the same time and used AMeDAS
142 surface wind data and made a hypothesis that Suzuka-oroshi was downslope-windstorms
143 with hydraulic jumps and gap-winds. They observed the downslope winds but were not able
144 to observe the gap winds. Therefore, it remains unclear whether Suzuka-oroshi is the
145 downslope windstorms or the gap-winds.

146 Based on previous studies, the current study was performed to determine where the
147 Suzuka-oroshi winds blow strongly, the favorable atmospheric conditions for the formation
148 of Suzuka-oroshi, and the major formation mechanism of the Suzuka-oroshi, either
149 downslope-windstorms or gap-winds.

150

151 **2 Data and Method**

152 *2.1 Climatological analysis*

153 We identified Suzuka-oroshi as the wind direction of south-southwest to north-northwest
154 and a wind speed of 11 m s^{-1} or higher on the east side of the Suzuka Mountains, defined
155 as the time when the wind was blowing on the leeward side of the Suzuka Mountains. In
156 addition, we considered any continuous period during which Suzuka-oroshi was blowing as
157 a Suzuka-oroshi case. When the interruption time was less than 3 h, the interruption time
158 was ignored, and the data collected before and after the interruption were combined into
159 one case. The lower limit of wind speed for Suzuka-oroshi was set to match the reported
160 feelings of local residents, as local winds are recognized and named by the people living in

161 the area. Therefore, we first interviewed the local residents, which revealed that strong wind
162 causing the power lines to roar and inducing fear in people are named as Suzuka-oroshi.
163 This feeling is expressed using the Beaufort Scale: strong breeze, wind speed 10.8–13.8 m
164 s⁻¹ at 10 m above ground. Therefore, we set 11 m s⁻¹ as the lower limit of the wind speed of
165 Suzuka-oroshi. In addition, to compare our results with those of previous studies, a Weak-
166 Suzuka-oroshi was extracted under a wind speed of 8 m s⁻¹ and analyzed using the same
167 approach as used for Suzuka-oroshi with more than 11 m s⁻¹ wind speed.

168 However, because the installation heights of the anemometers differed at each
169 observation point, the wind speed observed at each location was converted to the wind
170 speed at 10 m above ground level using the following power-law formula (Eq. (2)):

$$171 \quad U_{10} = U_z(10/Z)^\alpha \quad (2)$$

172 Here, U_{10} is the wind speed at 10 m above ground, U_z is the observed wind speed, z is
173 the observed height, and α is a parameter representing the surface roughness and
174 atmospheric stability in the surface layer. The α was set to 0.25, which is used for winds over
175 forests, urban areas without tall buildings, and residential areas (Wind Engineering
176 Research Institute, 1984). Unless otherwise noted, the surface wind speed was defined as
177 the wind speed at 10 m above ground level. The surface observation data are summarized
178 in Fig. 1 and Table 1. In addition to data from the Japan Meteorological Agency's AMeDAS,
179 we used the Ministry of the Environment's data (Atmospheric Environmental Regional
180 Observation System) and the data observed at highways. The data period was from January

181 1, 2012, to December 31, 2016, with data intervals of 10 minutes for AMeDAS and
182 Atmospheric Environmental Regional Observation System and 5 minutes for highways.

183 We first investigated the spatial distribution of Suzuka-oroshi and then surveyed a
184 typical weather pattern when Suzuka-oroshi was blowing. Seasonal and time-dependent
185 characteristics of Suzuka-oroshi were also investigated. Third, we examined the location at
186 which the Suzuka-oroshi occurred. Finally, we investigated the presence or absence of an
187 inversion layer using radiosonde observation data at Wajima, the location of which is shown
188 in Fig. 1. At Wajima observatory, Sonde observations are performed at 0900 and 2100 Japan
189 Standard Time (JST). We defined an inversion layer as any layer in which the temperature
190 increases as the altitude rises at 1–5 km level in the sonde data. The wind speed
191 approaching the mountains was calculated using the westerly wind component at the 950
192 hPa level over the windward mountains shown in Fig. 1 as blue square just before or just
193 after the onset of Suzuka-oroshi. As the wind component, we used mesoscale analysis data
194 with horizontal resolutions of 5 km and time resolutions of 3 hours, provided by Japan
195 Meteorological Agency (JMA).

196

197 *2.2 Numerical simulations*

198 To further investigate the effects of the Suzuka Mountains on Suzuka-oroshi events, we
199 conducted numerical simulations using the Weather Research and Forecasting (WRF)
200 model, covering a case that occurred on March 5–6, 2014, which was named as the CTRL.

201 We also simulated a case in which the Suzuka Mountains were excluded from the
202 topographic data, named as case NoMt. Fig. 3 shows the simulation domain and
203 topographic settings of the two simulation cases. The domain consists of 398×648 grid
204 points with a horizontal grid spacing of 1.0 km. The domains have 50 vertical sigma levels,
205 and the model top is 100 hPa. The initial and boundary conditions were obtained from
206 mesoscale analysis data. The model configurations are summarized in Table 2.

207

208 **3 Results**

209 *3.1 Climatological analysis*

210 Fig. 2 shows typical weather patterns when the Suzuka-oroshi was blowing. Suzuka-
211 oroshi tended to occur when an extratropical cyclone with a cold front passed over the Sea
212 of Japan (Fig. 2c). This was the primary weather pattern in 27 cases (55% of cases) (Table
213 3). The second typical weather pattern is an extratropical cyclone type but is located offshore
214 of Kanto and Sanriku (Fig. 2a), which comprised seven cases (16% of cases). Other types
215 of weather patterns included the typhoon type (Fig. 2e). In contrast, the primary weather
216 pattern of the Weak-Suzuka-oroshi is an extratropical cyclone located offshore of Kanto and
217 Sanriku (Fig. 2a). This type accounts for 147 cases (36% of cases).

218 Fig. 4 shows the seasonal and time-dependent characteristics of the Suzuka-oroshi. As
219 shown in Fig. 4a, the frequency of Suzuka-oroshi was highest in spring (March to April) and
220 lowest in summer (June to August), although the sample size may not be large enough. In

221 Japan, extratropical cyclones and associated cold fronts often pass through these areas in
222 spring. The frequency of Weak-Suzuka-oroshi supports the tendency in Owada (1990) (Fig.
223 4b). Suzuka-oroshi tended to occur in the late afternoon, but this time dependency was
224 weaker than that of Weak-Suzuka-oroshi (Fig. 4c, d).

225 We then examined the location at which Suzuka-oroshi tended to blow. The results of
226 the climatological survey (Fig. 5a, b) showed that in the northern part of the plain, Suzuka-
227 oroshi blows most frequently around Komono, which is inland at the foothills of the Suzuka
228 Mountains. It rarely blows near the northern part of the plain along the coast. In the southern
229 and central parts, it blows anywhere. In addition, the wind direction was mostly northwest at
230 most locations during Suzuka-oroshi events. On the other hand, Weak-Suzuka-oroshi
231 occurs anywhere on the plain (Fig. 5c, d).

232 We also compared the wind speeds on the windward and leeward sides of the Suzuka
233 Mountains during Suzuka-oroshi events; the results are shown in Fig. 6. The mean wind
234 speed was approximately 5 m s^{-1} higher at Tsu on the leeward side of the mountains than at
235 Higashiomi on the windward side. Thus, the wind speed may increase after passing over
236 the mountains. In contrast, in the case of Weak-Suzuka-oroshi, the difference in wind speed
237 between the windward and leeward mountains was small. These results suggest that the
238 presence of the mountains is responsible for the strong winds of Suzuka-oroshi.

239 However, this does not reveal whether Suzuka-oroshi is a downslope wind. Therefore,
240 we investigated whether the environmental field during the Suzuka-oroshi event was

241 favorable for generating downslope windstorms.

242 Table 4 shows that an inversion layer at 1-5 km level was present in 31 Suzuka-oroshi
243 cases (74% of cases). This result is consistent with the tendency of weather patterns in
244 which Suzuka-oroshi often occurs when an extratropical cyclone with a cold front passes
245 over the Sea of Japan. The wind speed approaching the mountains ranged from 6 to 12 m
246 s^{-1} in 23 cases (55% of cases). On the other hand, there were nine cases (21% of cases) in
247 which there was no inversion layer at 1-5 km. We calculated Fr in these four cases, using
248 the wind speed data, Brunt- Väisälä frequency N , and the mountain height H that was set to
249 1000 m. Fr values were 0.8–1.4, which is favorable for the downslope windstorms. Thus,
250 most Suzuka-oroshi cases occurred under favorable atmospheric conditions for downslope
251 windstorms.

252

253 *3.2 Numerical simulations*

254 The simulation case was a strong wind event on March 5, 2014, which is a typical case
255 during a cyclone with a cold front was passing over the Sea of Japan (Fig. 7). There was no
256 inversion layer but a slightly strong stable layer around 1.5–2.0 km at the windward side
257 during the events. The inflow wind speed was within 6–12 $m s^{-1}$.

258 First, we confirmed the reproducibility of the temporal variations in the wind direction
259 and speed obtained from the CTRL simulation. We included the results of the comparison
260 at Tsu and Komono, where strong winds were observed. Fig. 8 shows that the wind speed

261 suddenly increased around 1600JST on March 5, 2014, at which time the 10-min average
262 wind speed exceeded 11 m s^{-1} . The time series of the observed wind direction shows that
263 the wind direction varied before the strong winds blew; however, after the strong winds
264 began blowing, the wind direction remained stable in the northwest. This time-series
265 variation is characteristic of downslope windstorms. Comparison of the simulated results
266 with the observations showed that the WRF model could reproduce the characteristics of
267 the observed time series of surface winds.

268 Second, we examined the reproducibility of the spatial distribution of surface winds
269 obtained from the CTRL simulation. The observations indicate that northwesterly strong
270 winds blew in the southern and central parts of the plains and northern foothills area (Fig.
271 9a). There were weaker wind areas in the northern part of the plain near the coast than
272 surroundings.

273 The numerical simulation results showed that overall, the simulated wind speed was
274 slightly higher than the observed speed (Fig. 9b). However, strong wind areas in the central
275 and southern parts of the plains and northern area near the foothills were well-represented.
276 The WRF model also reproduced the spatial characteristics of the winds observed at the
277 time the strong winds began to blow. Comparison results at other times are shown in
278 Appendix A.

279 After confirming that the WRF model reproduced the actual wind conditions, we
280 investigated the vertical structure of Suzuka-oroshi using the simulation results. Fig. 10

281 shows the temporal variation in the vertical cross-section of the potential temperature across
282 the northern part of the mountains. At 1300 JST, a relatively strong stable layer flowed into
283 the area at around 1.5–2 km altitude on the windward side (Fig. 10b). Simultaneously, a
284 relatively weak wind region formed over the leeward slope of the Suzuka Mountains, and
285 the isotherms decreased. From 1400 to 1500 JST, the amplitude of the mountain waves
286 increased, creating flows that split the previously formed weak wind region up and down
287 (Fig. 10c, d). The wind speed windward far from the mountains and on the leeward slopes
288 gradually increased from 1500 to 1600 JST (Fig. 10d, e). Based on the vertical cross-section
289 at the time when the surface wind speed was the highest, the isentropes were largely drawn
290 down along the leeward slope, and the wind speed in this direction increased by
291 approximately 5 m s^{-1} compared to that in the windward direction (Fig. 10e). At 1300-1600
292 JST, it seems that the flow undergoes a transition from subcritical on the windward side to
293 supercritical flow on the lee slope. Indeed, internal Froude number ($Fi = U/\sqrt{g^*h}$) was less
294 than 1.0 (approximately 0.5-0.8) at the windward and larger than 1.0 (approximately 1.6-2.9)
295 above the leeward slope from 1300 to 1600 JST. Here, U and h are wind speed and depth
296 of the duct (or inversion layer height), respectively. g^* is reduced gravity constant,
297 considering the potential temperature difference between the two layers ($g^* = \frac{\Delta\theta}{\theta}g$). In the
298 leeward region of the mountains, the airflow jumps slightly on the ground level, and the ridge
299 is located near the coast. A weak wind area near the ground level was generated in response
300 to this ridge of mountain waves. In addition, there was a relatively weaker wind region with

301 a large wave amplitude above the strong wind layer. These results reflect the general
302 characteristics of downslope windstorms. After that, as the inflow wind speed increased, the
303 overall surface wind speed increased until 0000 JST on March 6, 2014, and then gradually
304 decreased.

305 On the other hand, the vertical cross-sections of the central and southern regions
306 showed that the isentropes were not largely drawn down along the leeward slope of the
307 mountains (Fig. 11). As a result, the isotherms below 1 km altitude are not so dense over
308 the leeward slope and plain. It is considered that the wind speed between the north and
309 south parts differed because of differences in height of the mountains.

310 Fig. 12 shows the distribution of deviations in the surface wind speed simulated from
311 the CTRL case minus the results of the NoMt case. The presence of the Suzuka Mountains
312 strengthened the surface wind speeds by approximately 4–6 m s⁻¹ leeward of the mountains.
313 Fig. 10 and Fig. 12 show that the Suzuka-oroshi were downslope winds caused by the
314 topographic effect of the Suzuka Mountains.

315

316 **4 Discussion**

317 We found that the Suzuka-oroshi blow not only in the southern part of the plain on the
318 leeward side of the Suzuka Mountains, but also in the northern and central parts. This finding
319 is consistent with anecdotal observations from local residents. The reasons for the difference
320 in the strong-wind areas found in this study compared to those of previous studies may be

321 as follows: Owada (1990) did not survey the northern part of the plain leeward of the Suzuka
322 Mountains. Additionally, Komatsu and Tachibana (2016) did not survey winds in the northern
323 part of the plain near the mountain foothills. In the central part of the plain, they did not
324 consider differences in the above-ground level of the AMeDAS anemometers at different
325 observation stations. The AMeDAS anemometers installed in the central part are
326 approximately 10 m lower than those installed in the southern part. This difference in height
327 leads to underestimation of the wind speeds by 3 m s^{-1} in the central part of the plain, which
328 may have prevented detection of strong winds in the central part of the plain by Komatsu
329 and Tachibana (2016).

330 The results of climatological analysis indicated that the atmospheric conditions were
331 suitable for generating downslope winds in many Suzuka-oroshi events. When an inversion
332 layer is present, downslope winds tend to occur, as described in Section 1. Note that the
333 inversion layer is supportive factor. If Fr is 0.6–1.2, the downslope windstorms tend to occur
334 even when an inversion layer is not present. (Lin and Wang 1996).

335 The results of the numerical simulation also revealed a slightly strong stable layer
336 between 1.5–2.0 km levels in the windward and mountain ranges. Additionally, there were
337 large-amplitude of mountain waves and weaker wind layer above the leeward slope of the
338 Suzuka Mountains than surroundings; airflow below this weak wind region resulted in strong
339 winds. Note that this weak wind region was not a typical mountain-wave breaking region
340 above the mountain slope and did not develop a clear hydraulic jump. Such atmospheric

341 conditions cannot lead to formation of gusty, very strong downslope windstorms such as the
342 chinook and Yamaji-kaze but can cause strong winds due to the transition of the flow regime,
343 as shown by Durran (1990). Indeed, Suzuka-oroshi winds are stronger than the winds in
344 windward areas but are not similar to chinook. The simulation results from the CTRL and
345 NoMt cases supported the mountain effects on the strong winds and that the Suzuka-oroshi
346 exhibits characteristics of downslope windstorms. The pre-existing or self-induced critical
347 layer was not observed at the upper level (see figure in Appendix B). Thus, the Suzuka-
348 oroshi of this case does not support the resonant amplification theory.

349 We simulated Suzuka-oroshi in only one case and discussed the mechanism. To
350 improve the robustness of our results, additional cases should be evaluated. Particularly,
351 the mechanism of Suzuka-oroshi with a clear inversion layer was not investigated in the
352 simulations but will be examined in our further research.

353

354 **5 Conclusions**

355 The Suzuka-oroshi blow in the southern parts of the plain on the leeward side of the
356 Suzuka Mountains as well as in the northern part. The winds are strongest and more
357 frequent near the foot of the mountain range in the northern part. These results differed from
358 those of previous studies.

359 Suzuka-oroshi mainly occurs just after an extratropical cyclone with a cold front passing
360 through the Sea of Japan (55% of cases). Furthermore, an inversion layer at 1-5 km was

361 found in 74% of cases. Considering that Suzuka-oroshi tended to blow immediately after the
362 passages of cold fronts, this inversion layer may be a frontal inversion layer. The Suzuka-
363 oroshi also blow at night.

364 Numerical simulations with the high-resolution Weather Research and Forecasting
365 (WRF) model supported this finding. Simulation results with and without the Suzuka
366 Mountains demonstrated that the strong Suzuka-oroshi in the northern part of the plain
367 comprised downslope windstorms with transition of flow regime. Additionally, differences in
368 height of the mountains between the north and south parts results in the greater wind speed
369 in the northern parts compared to the southern parts.

370 We determined the location, timing, and reasons for Suzuka-oroshi blowing. These
371 results improve the understanding of local winds in Japan and may contribute to the safe
372 operation and management of highways in this region.

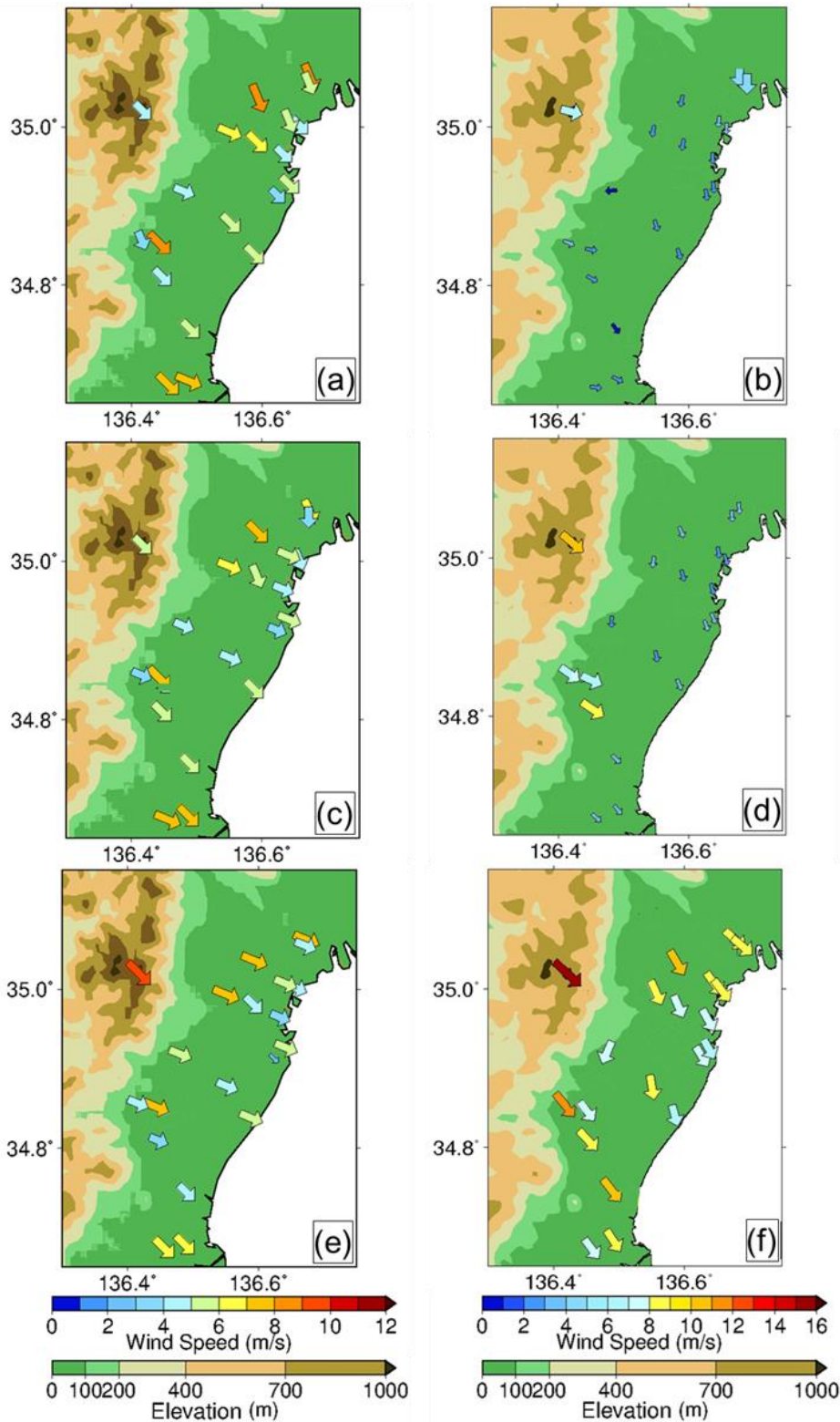
373

374 **Acknowledgments**

375 This research was supported by the Environment Research and Technology Development
376 Fund JPMEERF20192005 of the Environmental Restoration and Conservation Agency of
377 Japan. This research was supported by the Multidisciplinary Cooperative Research Program
378 of the Center for Computational Sciences, University of Tsukuba.

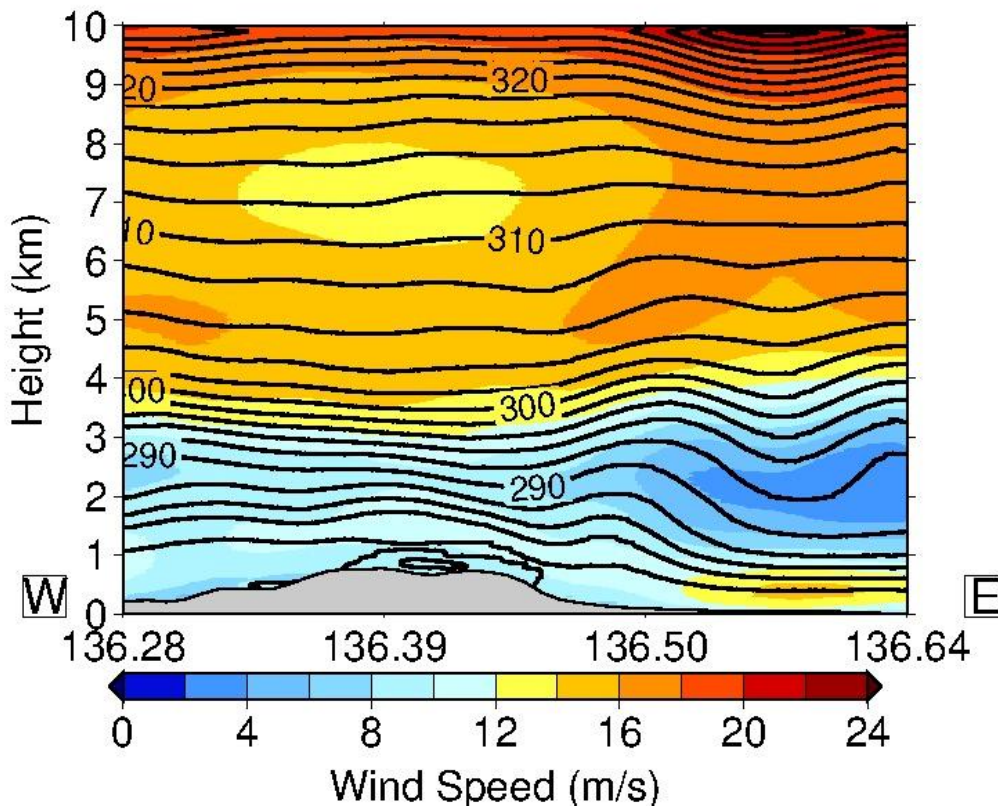
379 **Appendix A**

380 Distribution of surface winds leeward of the Suzuka Mountains. Results from observations
381 on March 5, 2014, at (a) 1200 JST, (c) 1400 JST, (e) 1600 JST. Results from CTRL simulation
382 on March 5, 2014, at (b) 1200 JST, (d) 1400 JST, (f) 1600 JST.



383 **Appendix B**

384 Vertical cross section of wind speed to 10 km altitude from CTRL simulation across the
385 northern Suzuka Mountains (line A in Fig. 3) at 1600 JST on March 5, 2014 (CTRL
386 simulation). Shade and contour indicate horizontal wind speed (m/s) and potential
387 temperature (K), respectively.



388

389 **Data Availability Statements**

390 The datasets generated in this study will be available from the corresponding author upon
391 reasonable request for the next five years.

392 **References**

393 Arakawa, S., 1968: A proposed mechanism of fall winds and Dashikaze. *Pap. Meteor.*

394 *Geophys* 19, 69-99.

395 Arakawa, S., 1969: Climatological and dynamic studies on the local strong winds, mainly in

396 Hokkaido, Japan. *Geophys. Mag.* 34 359-425.

397 Armi, L., and G. J. Mayr, 2007: Stratified flow across an Alpine crest with a pass: Shallow

398 and deep flows. *Quart. J. Roy. Met. Soc.*, 133, 459-477.

399 Asano, Y., and H. Kusaka, 2022: Numerical simulation study of the effects of foehn winds

400 on white head incidences in Yamagata Prefecture, Japan. *Meteorological Applications*. (in

401 press)

402 Durran, D. R., 1986: Mountain waves. *Mesoscale meteorology and forecasting*. American

403 Meteorological Society, Boston, MA, 472-492.

404 Durran, D. R., and J. B. Klemp, 1987: Another look at downslope winds. Part II: Nonlinear

405 amplification beneath wave-overturning layers. *Journal of Atmospheric Sciences* 44(22)

406 3402-3412.

407 Durran, D. R., 1990: Mountain waves and downslope winds. *Atmospheric processes over*

408 *complex terrain*. American Meteorological Society, Boston, MA, 23(45), 59-81.

409 Elvidge, A. D., and I. A. Renfrew, 2016: The causes of foehn warming in the lee of mountains.

410 *Bull. Amer. Meteor. Soc.*, 97(3), 455– 466.

411 Elvidge, A.D., I. A. Renfrew, J. C. King, A. Orr, and T. A. Lachlan-Cope, 2016: Foehn warming

412 distributions in non-linear and linear flow regimes: A focus on the Antarctic Peninsula.
413 *Quarterly Journal of the Royal Meteorological Society*, 142(695), 618–631.

414 Elvidge, A.D., P. K. Munneke, J. C. King, I. A. Renfrew, and E. Gilbert, 2020: Atmospheric
415 drivers of melt on Larsen C ice shelf: surface energy budget regimes and the impact of
416 foehn. *Journal of Geophysical Research. Atmospheres*, 125(17), e2020JD032463.

417 Fudeyasu, H., T. Kuwagata, Y. Ohashi, S. I. Suzuki, Y. Kiyohara, and Y. Hozumi, 2008:
418 Numerical study of the local downslope wind “Hirodo-Kaze” in Japan. *Mon. Wea. Rev.*
419 136(1), 27-40.

420 Gaberšek, S., and D. R. Durran, 2004: Gap flows through idealized topography. Part II:
421 Effects of rotation and surface friction. *J. Atmos. Sci.*, 63, 2720-2739.

422 Glenn, C. L., 1961: The Chinook, *Wetherwise*, 14,174 -182.

423 Gohm, A., and G. J. Mayr, 2004: Hydraulic aspects of foehn winds in an Alpine valley. *Quart.*
424 *J. Roy. Met. Soc.*, 130, 449-480.

425 Gohm, A., and G. J. Mayr, 2005: Numerical and observational case-study of a deep Adriatic
426 bora. *Quart. J. Roy. Met. Soc.*, 131, 1363-1392.

427 Gohm, A., G. Mayr, A. Fix, and A. Giez, 2008: On the onset of bora and the formation of
428 rotors and jumps near a mountain gap. *Quart. J. Roy. Met. Soc.*, 134, 21-46.

429 Houghton, D. D., and A. Kasahara, 1968: Nonlinear shallow fluid flow over an isolated ridge.
430 *Communications on Pure and Applied Mathematics*, 21(1), 1-23.

431 Ishii, S., K. Sasaki, K. Mizutani, T. Aoki, T. Itabe, H. Kanno, D. Matsushima, W. Sha, A. T.

432 Noda, M. Sawada, M. Ujiie, Y. Matsuura, and T. Iwasaki, 2007: Temporal evolution and
433 spatial structure of the local easterly wind "Kiyokawa-dashi" in Japan PART I: Coherent
434 Doppler lidar observations. *Journal of the Meteorological Society of Japan*. II 85 797-813.

435 Klemp, J. B., and D. R. Lilly, 1975: The dynamics of wave-induced downslope winds. *Journal*
436 *of Atmospheric Sciences* 32(2) 320-339.

437 Klemp, J. B., and D. R. Durran, 1987: Numerical modeling of Bora winds. *Meteorol. Atmos.*
438 *Phys.*, 36, 215-227.

439 Komatsu, K. K., and Y. Tachibana, 2016: Two types of strong local wind captured by
440 simultaneous multiple-site radiosonde soundings across a mountain range. *Mon. Wea.*
441 *Rev.*, 144, 3915-3936.

442 Koyanagi, T., and H. Kusaka, 2020: A climatological study of the strongest local winds of
443 Japan "Inami-kaze". *Int. J. Climatol.*, 40(2), 1007-1021.

444 Kusaka, H., Y. Miya, and R. Ikeda, 2011: Effects of solar radiation amount and synoptic-
445 scale wind on the local wind "Karakkaze" over the Kanto Plain in Japan. *J. Meteor Soc.*
446 *Japan*, 89(4), 327-340.

447 Kusaka, H., and H. Fudeyasu, 2017: Review of downslope windstorms in Japan. *Wind* 286
448 *& Structures*, 24(6), 637-656.

449 Kusaka, H., A. Nishi, A. Kakinuma, Q. Doan, T Onodera, S. Endo, 2021: Japan's south foehn
450 on the Toyama Plain: Dynamical or thermodynamical mechanisms ?. *Int. J. Climatol.* DOI:
451 10.1002/joc.7133

452 Nishi, A., and H. Kusaka, 2019a: A Climatological Study of the Local “Karakkaze” Wind, with
453 a Focus on Temperature Change. *SOLA*, 15, 149-153.

454 Nishi, A., and H. Kusaka, 2019b: The “Karakkaze” Local Wind as a Convexity Wind: A Case
455 Study Using Dual-Sonde Observations and a Numerical Simulation. *SOLA*, 15, 160-165.

456 Lilly, D. K., and E. J. Zipser, 1972: The front range windstorm of 11 January 1972.
457 *Weatherwise*, 25, 56-63.

458 Lilly, D. K., and J. B. Klemp, 1979: The effects of terrain shape on nonlinear hydrostatic
459 mountain waves. *J. Fluid Mech.*, 95, 241–261.

460 Lin, Y. L., and T. A. Wang 1996: Flow regimes and transient dynamics of two-dimensional
461 stratified flow over an isolated mountain ridge. *J. Atmos. Sci.*, 53(1), 139-158.

462 Lin, Y. L., 2007: Mesoscale dynamics. Vol. 630. *Cambridge: Cambridge University Press*

463 Miller, P. P. and D. R. Durran, 1991: On the sensitivity of downslope windstorms to the
464 asymmetry of the mountain profiles. *J. Atmos. Sci.* 48, 1457–1473.

465 Orr, A., G. J. Marshall, J. C. Hunt, J. Sommeria, C. G. Wang, N. P. Van Lipzig, D. Cresswell,
466 and J. C. King, 2008: Characteristics of summer airflow over the Antarctic Peninsula in
467 response to recent strengthening of westerly circumpolar winds. *Journal of the*
468 *Atmospheric Sciences*, 65(4), 1396–1413.

469 Owada, M., 1990: A climatological study of local winds (oroshi) in central Japan. *Doctoral*
470 *Thes. Inst. Geosci., Univ. Tsukuba*, 98.

471 Pitts, R. O., and T. J. Lyons, 1989: Airflow over a two-dimensional escarpment. 1:

472 Observations. *Quart. J. Roy. Met. Soc.*, 115, 965-981.

473 Raymond, D., 1972: Calculation of airflow over an arbitrary ridge including diabatic heating
474 and cooling. *J. Atmos. Sci.*, 29, 837-843.

475 Saito, K., and M. Ikawa, 1991: A numerical study of the local downslope wind "Yamaji-kaze"
476 in Japan. *Journal of the Meteorological Society of Japan*. 69(1) 31-56.

477 Saito K., 1993: A Numerical Study of the Local Downslope Wind "Yamaji-kaze" in Japan. *J.*
478 *Meteor Soc. Japan*, 71(2), 247-272.

479 Saito, K., 1994 "A Numerical Study of the Local Downslope Wind"Yamaji -kaze" in Japan
480 Part 3: Numerical Simulation of the 27 September 1991 Windstorm with a Non-hydrostatic
481 Multi-nested Model", *J. Meteor Soc. Japan*, 72(2), pp.301-329.

482 Sasaki, K., H. Kanno, D. Matsushima, W. Sha, T. Iwasaki, S. Ishii, K. Mizutani, M. Moriyama,
483 K. Fukubori, M. Murai, and K. Yokoyama, 2005: An Observational Study of the Local
484 Easterly Strong Wind "Kiyokawa-dashi" in the Shonai Plains, Yamagata. *Journal of*
485 *Agricultural Meteorology* 60(5) 725-728.

486 Sasaki, K., M. Sawada, S. Ishii, H. Kanno, K. Mizutani, T. Aoki, T. Itabe, D. Matsushima, W.
487 Sha, A. T. Noda, M. Ujiie, Y. Matsuura, and T. Iwasaki, 2010: The temporal evolution and
488 spatial structure of the local easterly wind "Kiyokawa-dashi" in Japan. Part II: Numerical
489 simulations, *J. Meteorol. Soc. Japan*, 88(2), 161-181.

490 Sawada, M., T. Iwasaki, W. Sha, T. Yamazaki, H. Iwai, S. Ishii, K. Mizutani, and T. Itabe,
491 Transient downslope winds under the influence of stationary lee waves from the Zao

492 mountain range. *Journal of the Meteorological Society of Japan*. 90(1) 79-100.

493 Smith, R. B., 1985: On severe downslope winds. *J. Atmos. Sci.*, 42, 2597-2603.

494 Smith, R. B., 1987: Aerial observations of the Yugoslavian bora. *J. Atmos. Sci.*, 44, 269-297.

495 Smith, C. M., and E. D. Skillingstad, 2011: Effects of inversion height and surface heat flux
496 on downslope windstorms. *Mon. Wea. Rev.*, 139(12), 3750-3764.

497 Wind Engineering Institute, Co., Ltd., 1984: This is all you need to know about building wind
498 *Kajima Institute Publishing Co., Ltd.*, 22pp. (in Japanese).

499 Yoshino, M. M., 1975: Climate in a Small Area. *University of Tokyo Press*, Japan, 549pp.

500 Yoshino, M. M., 1986: Climate in a small area. *New Ed.* Chijin Shokan, 298 pp. (in Japanese).

501 Zängl, G., A. Gohm, and G. Geier, 2004: South foehn in the Wipp Valley - Innsbruck region:
502 Numerical simulations on the 24 October 1999 case (MAP-IOP 10). *Meteor. Atmos. Phys.*,
503 86, 213-243.

List of Figures

504

505

506 Fig. 1. Topography around the Suzuka Mountains and observation points for data used.

507 Fig. 2. Typical weather pattern when the Suzuka-oroshi blows. (a) Kanto-Sanriku offshore

508 extratropical cyclone type. (b) Hokkaido-Okhotsk extratropical cyclone type. (c)

509 Extratropical cyclone through Sea of Japan type. (d) High-pressure system

510 approaching type. (e) Typhoon type.

511 Fig. 3. Topography used in the numerical simulations. (a) Control experiment (Case CTRL).

512 (b) Experiment without Suzuka Mountains (Case NoMt).

513 Fig. 4. Frequency of Suzuka-oroshi events by month and time from 2012 to 2016. (a)

514 Monthly frequency of Suzuka-oroshi, (b) Monthly frequency of Weak-Suzuka-

515 oroshi, (c) Hourly frequency of Suzuka-oroshi, and (d) Hourly frequency of Weak-

516 Suzuka-oroshi.

517 Fig. 5. Map of the frequency of Suzuka-oroshi events and wind rose at each location. (a)

518 frequency of Suzuka-oroshi, (b) frequency of Weak-Suzuka-oroshi, (c) wind rose

519 of Suzuka-oroshi, and (d) wind rose of Weak-Suzuka-oroshi.

520 Fig. 6. Distribution of kernel density estimation of wind speeds at the same time in Tsu and

521 Higashiomi during the Suzuka-oroshi events. A darker color indicates a denser

522 sample. (a) Suzuka-oroshi and (b) Weak-Suzuka-oroshi.

523 Fig. 7. Surface weather chart on March 5, 2014. (a) 0900JST. (b) 2100JST.

524 Fig. 8. Time series graphs of surface wind on March 5–6, 2014. (a) Tsu (b) Komono.

525 Fig. 9. Distribution of surface winds leeward of the Suzuka Mountains. (a) Results from
526 observations at 1700 on March 5, 2014, JST. (b) Results from CTRL simulation at
527 1700 on March 5, 2014, JST.

528 Fig. 10. Vertical cross section of isentropes from CTRL simulation across the northern
529 Suzuka Mountains (line A in Fig. 3) on March 5, 2014 (CTRL simulation). (a) 1200
530 JST. (b) 1300 JST. (c) 1400 JST. (d) 1500 JST. (e) 1600 JST.

531 . Vertical cross section of isentropes from CTRL simulation across the southern Suzuka
532 Mountains (line B in Fig. 3) on March 5, 2014. (a) 1200JST. (b) 1300JST. (c)
533 1400JST. (d) 1500JST. (e) 1600JST.

534 Fig. 12. Impacts of mountains on the surface wind speed (cases CTRL - NoMt) at 1700 on
535 March 5, 2014, JST.

536

List of Tables

537

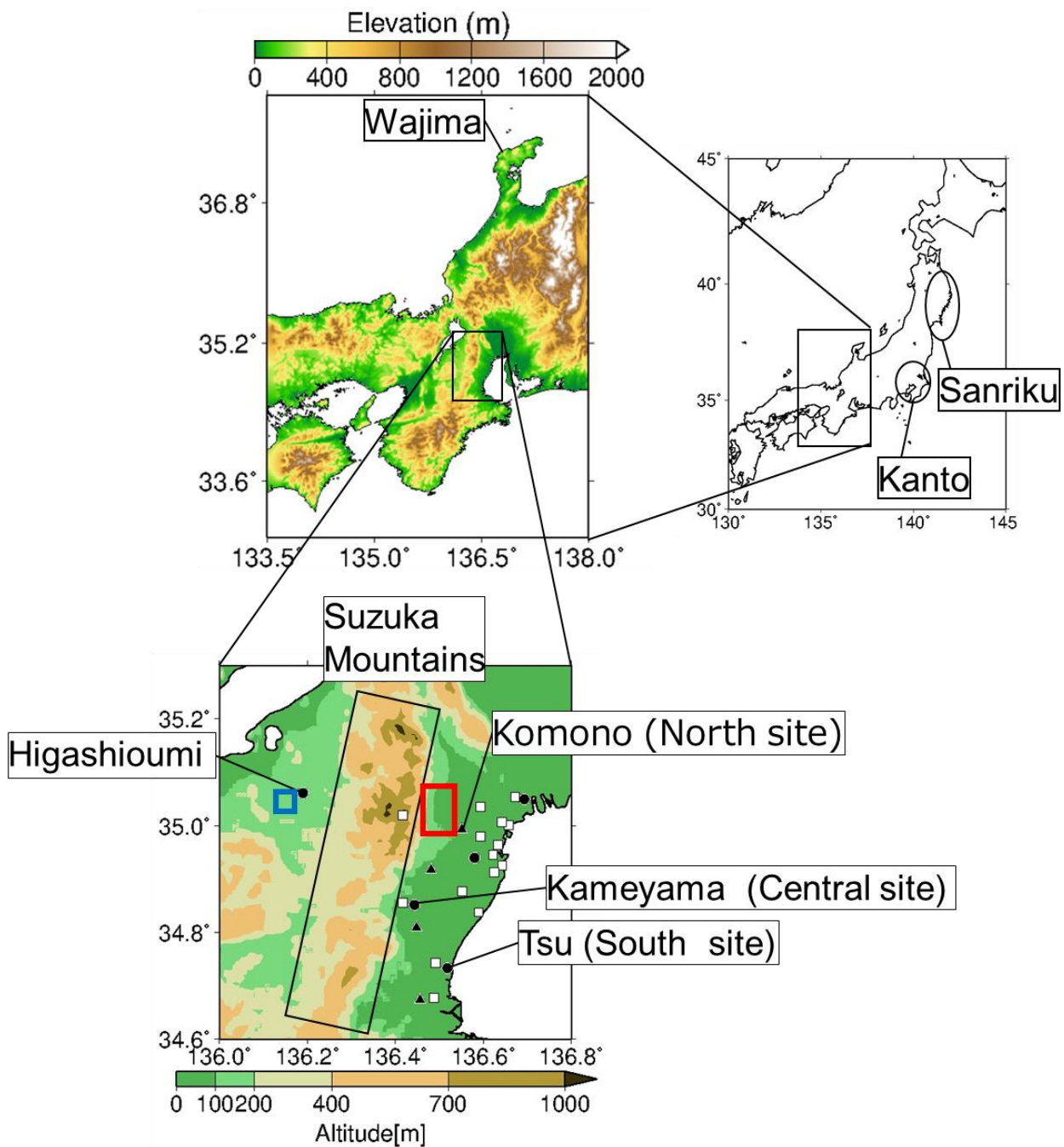
538 Table 1. Surface observation data.

539 Table 2. Model configuration.

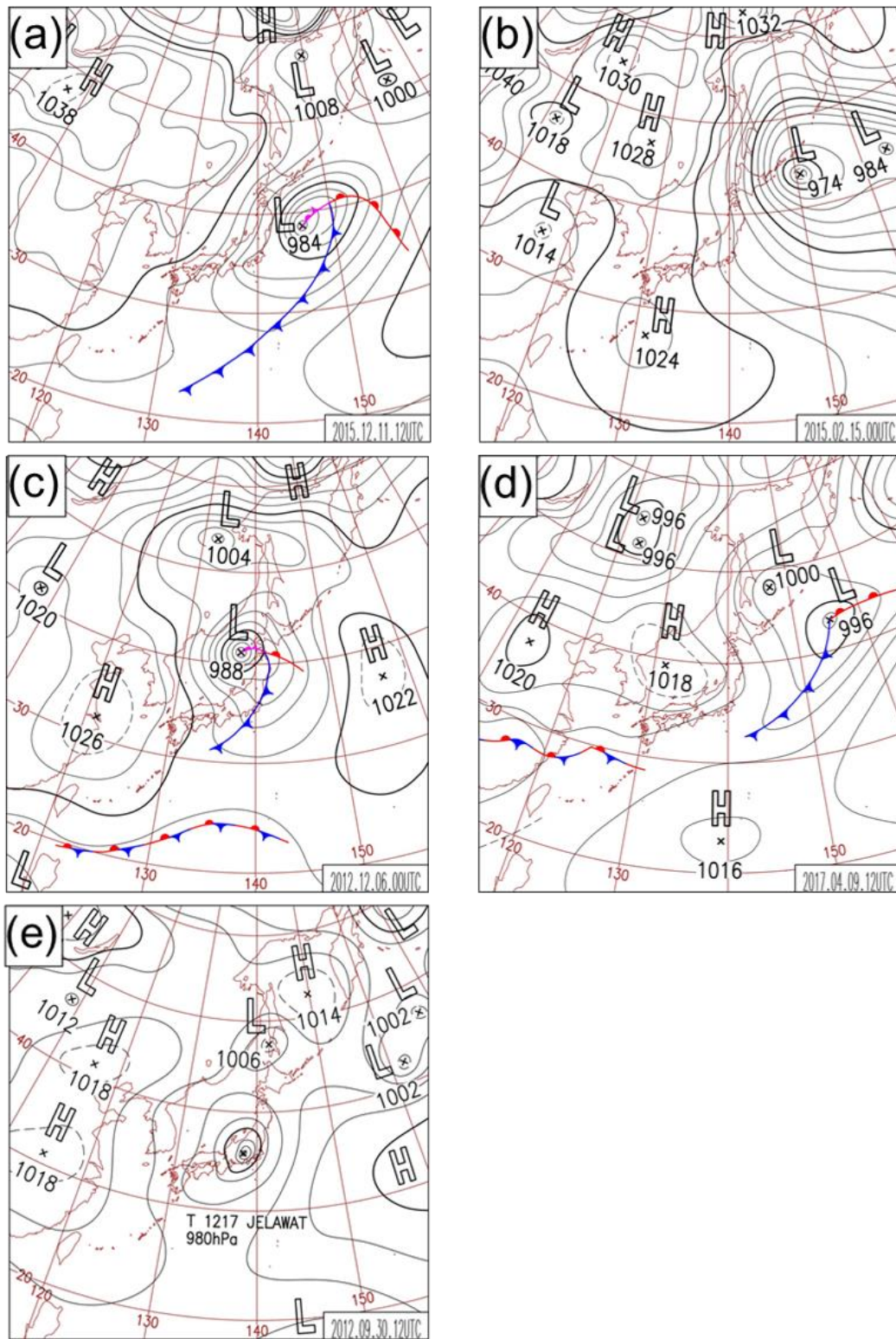
540 Table 3. Breakdown of typical weather patterns during Suzuka-oroshi events.

541 Table 4. Presence of inversion layer and wind speed approaching the mountains during

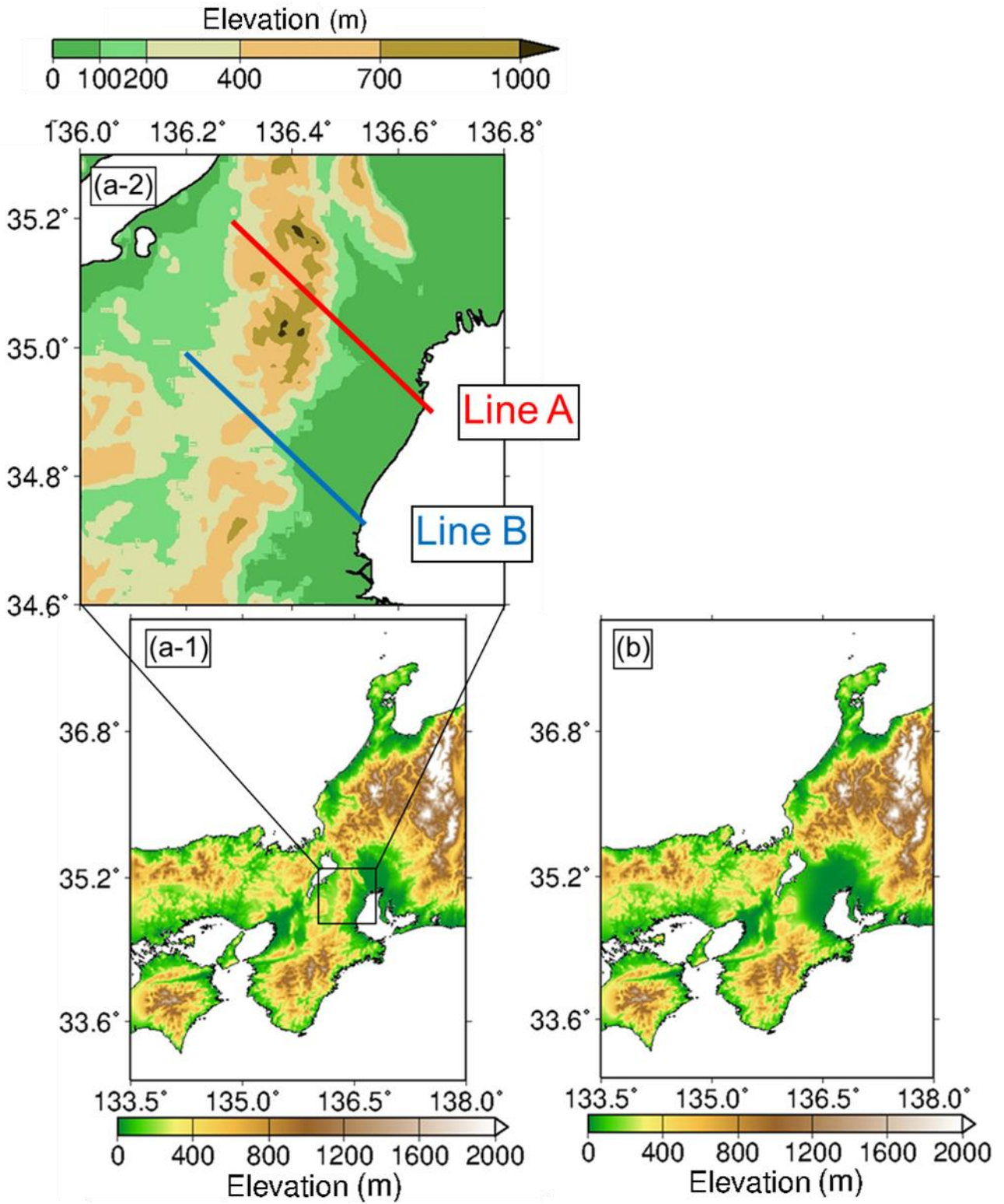
542 Suzuka-oroshi events.



543 Fig. 1. Topography around the Suzuka Mountains and observation points for data used.
 544 Black solid circles are AMeDAS, white solid squares are Atmospheric Environmental
 545 Regional Observation System and black solid triangles are observation points on the
 546 highways. Red square indicates the location of the local elementary school and fire
 547 department office. Blue square indicates the location of the data used as the wind speed
 548 approaching the mountains.

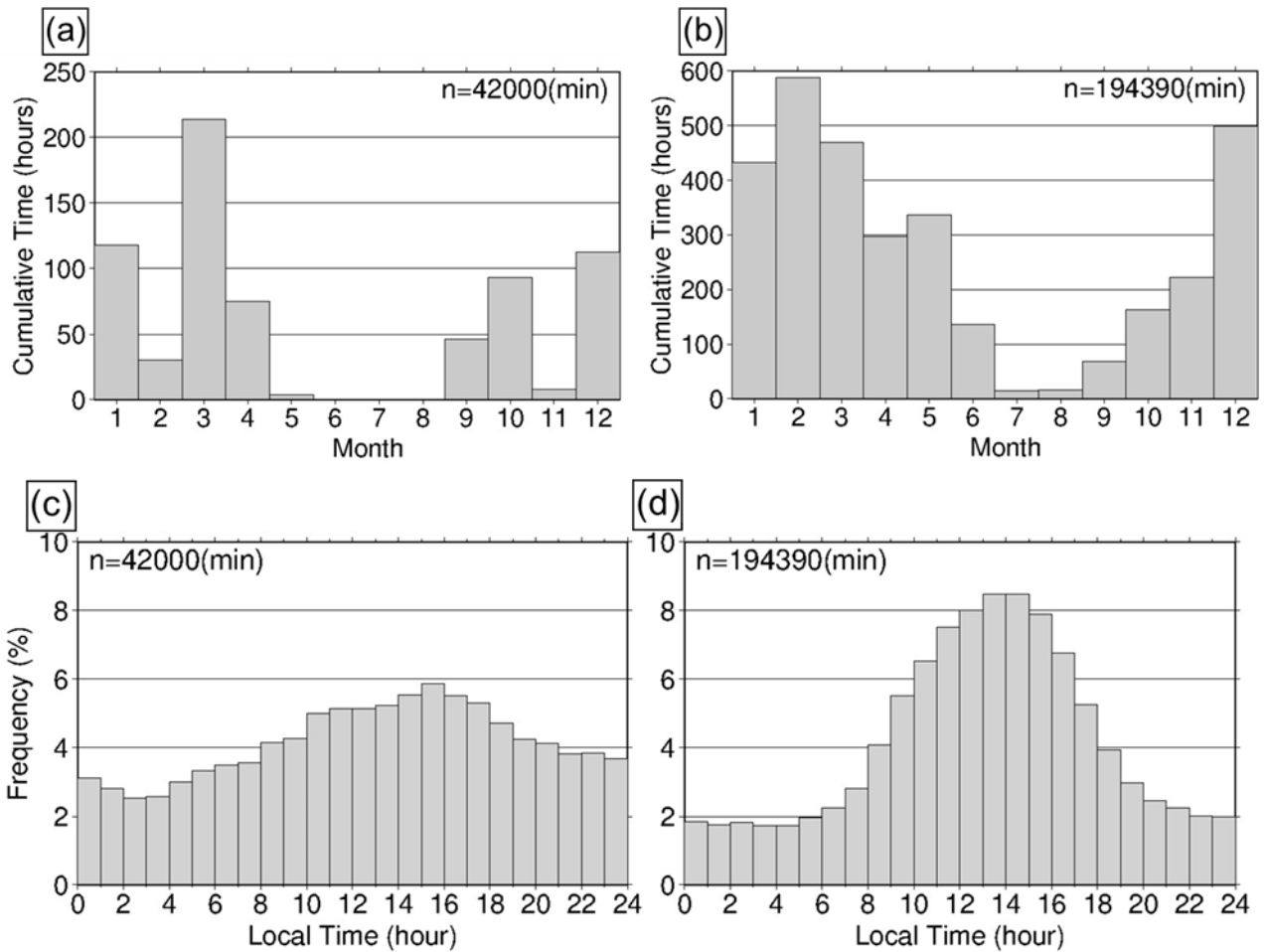


549 Fig. 2. Typical weather pattern when the Suzuka-oroshi blows. (a) Kanto-Sanriku offshore
 550 extratropical cyclone type. (b) Hokkaido-Okhotsk extratropical cyclone type. (c) Extratropical
 551 cyclone through Sea of Japan type. (d) High-pressure system approaching type. (e)
 552 Typhoon type.

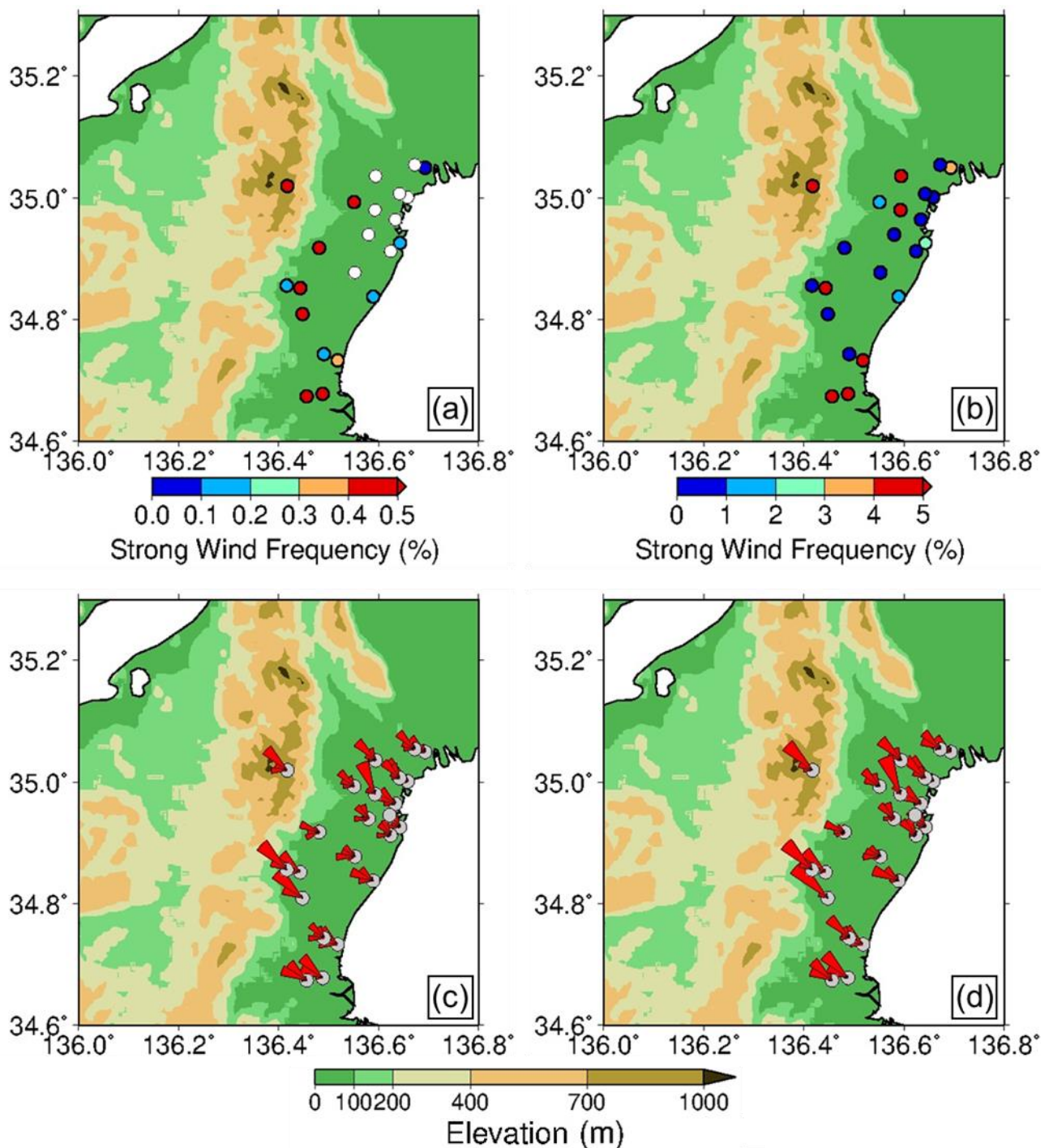


553 Fig. 3. Topography used in the numerical simulations. (a) Control experiment (Case CTRL).

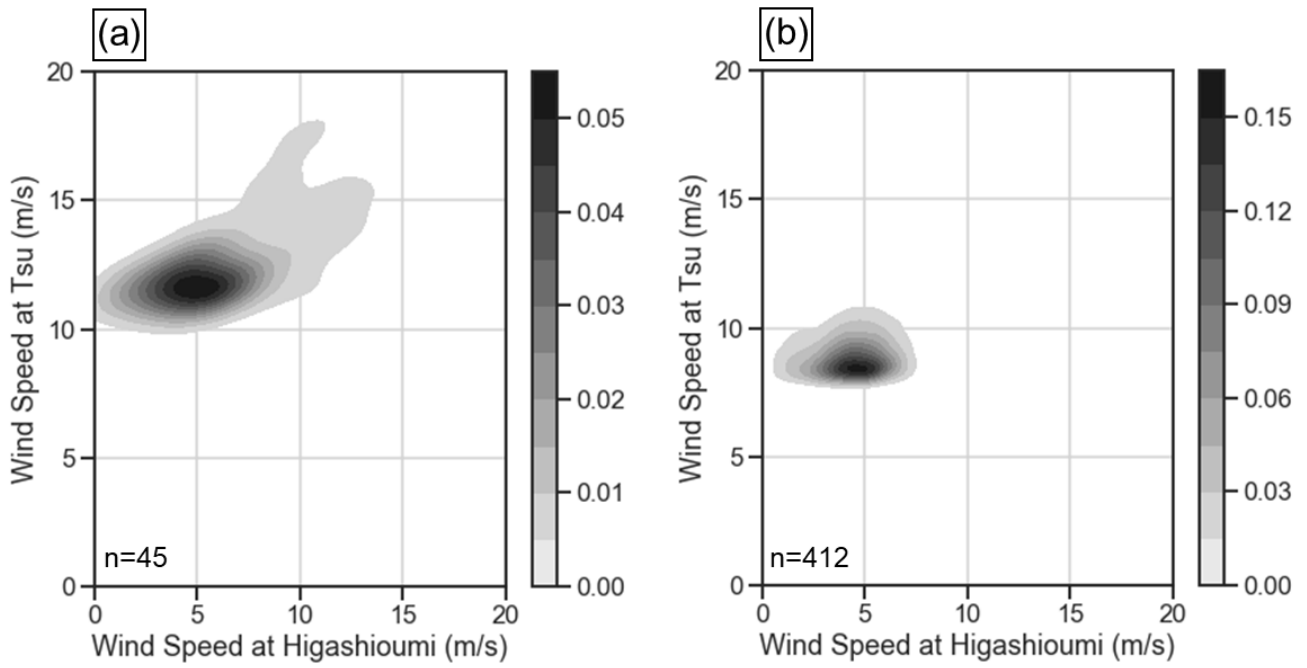
554 (b) Experiment without Suzuka Mountains (Case NoMt).



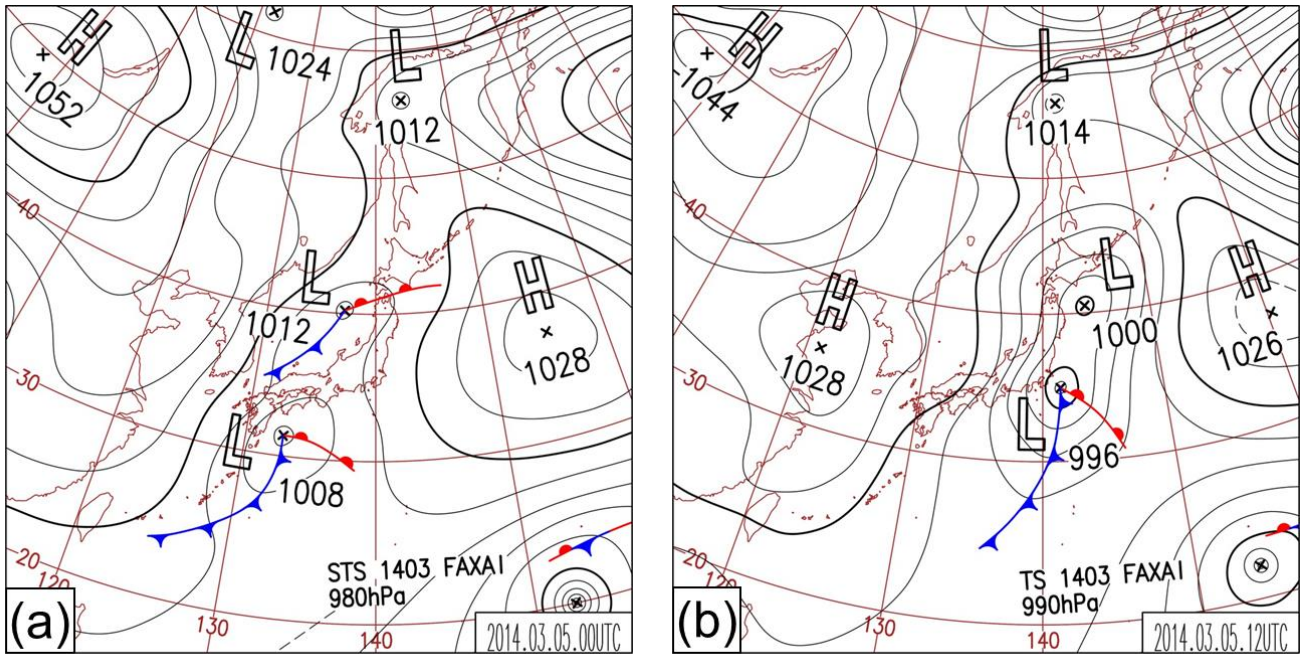
555 Fig. 4. Frequency of Suzuka-oroshi events by month and time from 2012 to 2016. (a)
 556 Monthly frequency of Suzuka-oroshi, (b) Monthly frequency of Weak-Suzuka-oroshi, (c)
 557 Hourly frequency of Suzuka-oroshi, and (d) Hourly frequency of Weak-Suzuka-oroshi. The
 558 time in the figure means Japan standard time (JST).



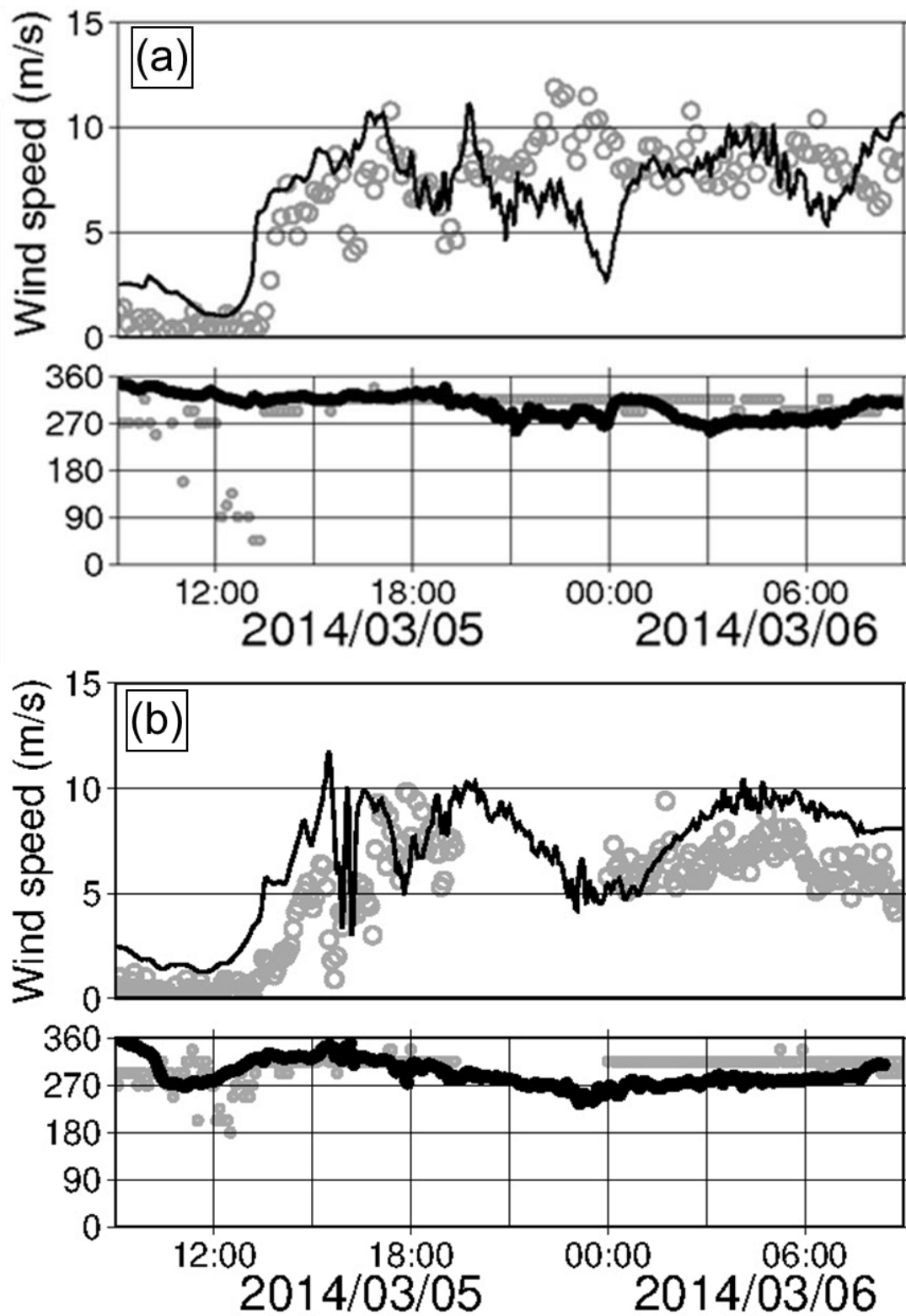
559 Fig. 5. Map of the frequency of Suzuka-oroshi events and wind rose at each location. (a)
 560 frequency of Suzuka-oroshi, (b) frequency of Weak-Suzuka-oroshi, (c) wind rose of Suzuka-
 561 oroshi, and (d) wind rose of Weak-Suzuka-oroshi. In (a) and (b), points shown by white
 562 circles indicate locations where Suzuka-oroshi events have never been observed. In (c) and
 563 (d), the longer the length of the fan, the more winds of that wind direction.



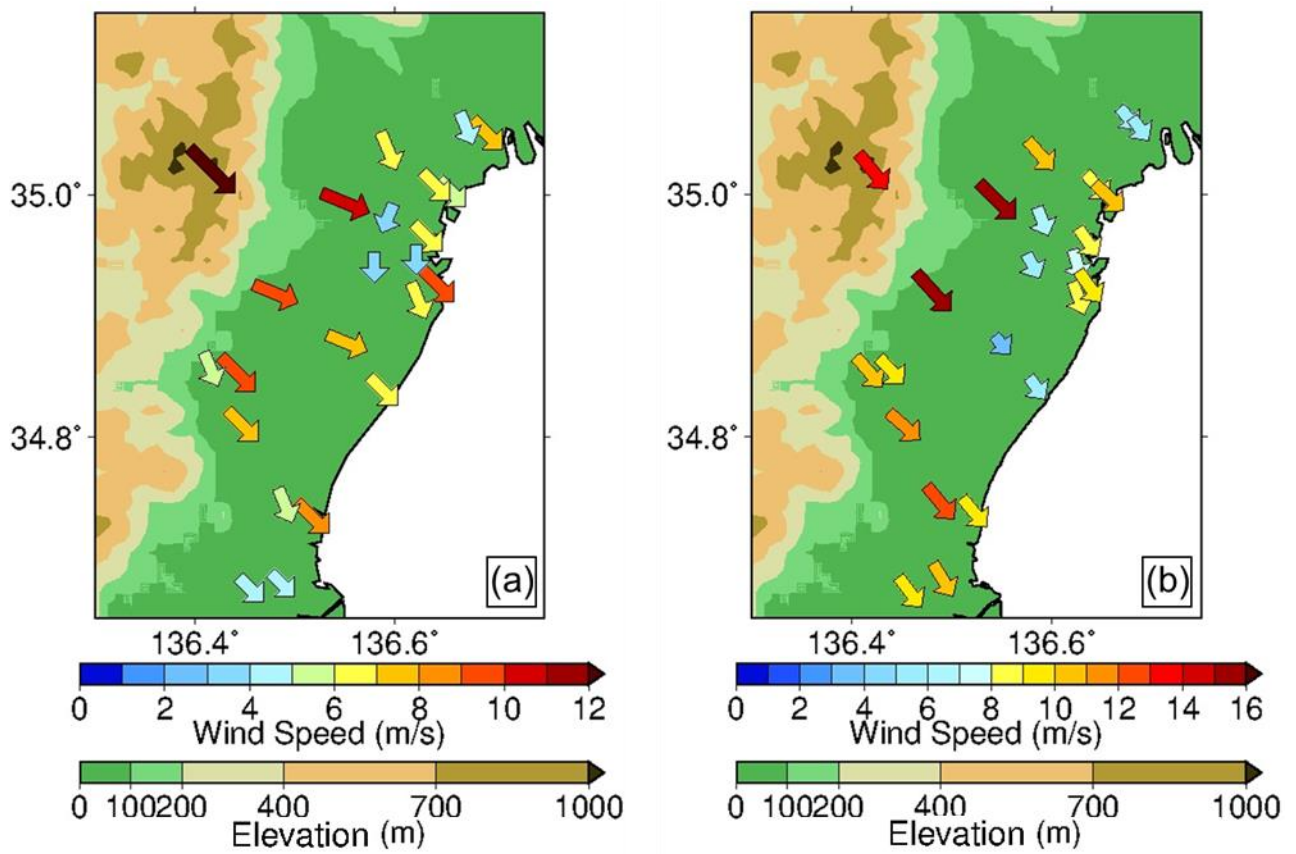
564 Fig. 6. Distribution of kernel density estimation of wind speeds at the same time in Tsu and
 565 Higashioumi during the Suzuka-oroshi events. A darker color indicates a denser sample. (a)
 566 Suzuka-oroshi and (b) Weak-Suzuka-oroshi.



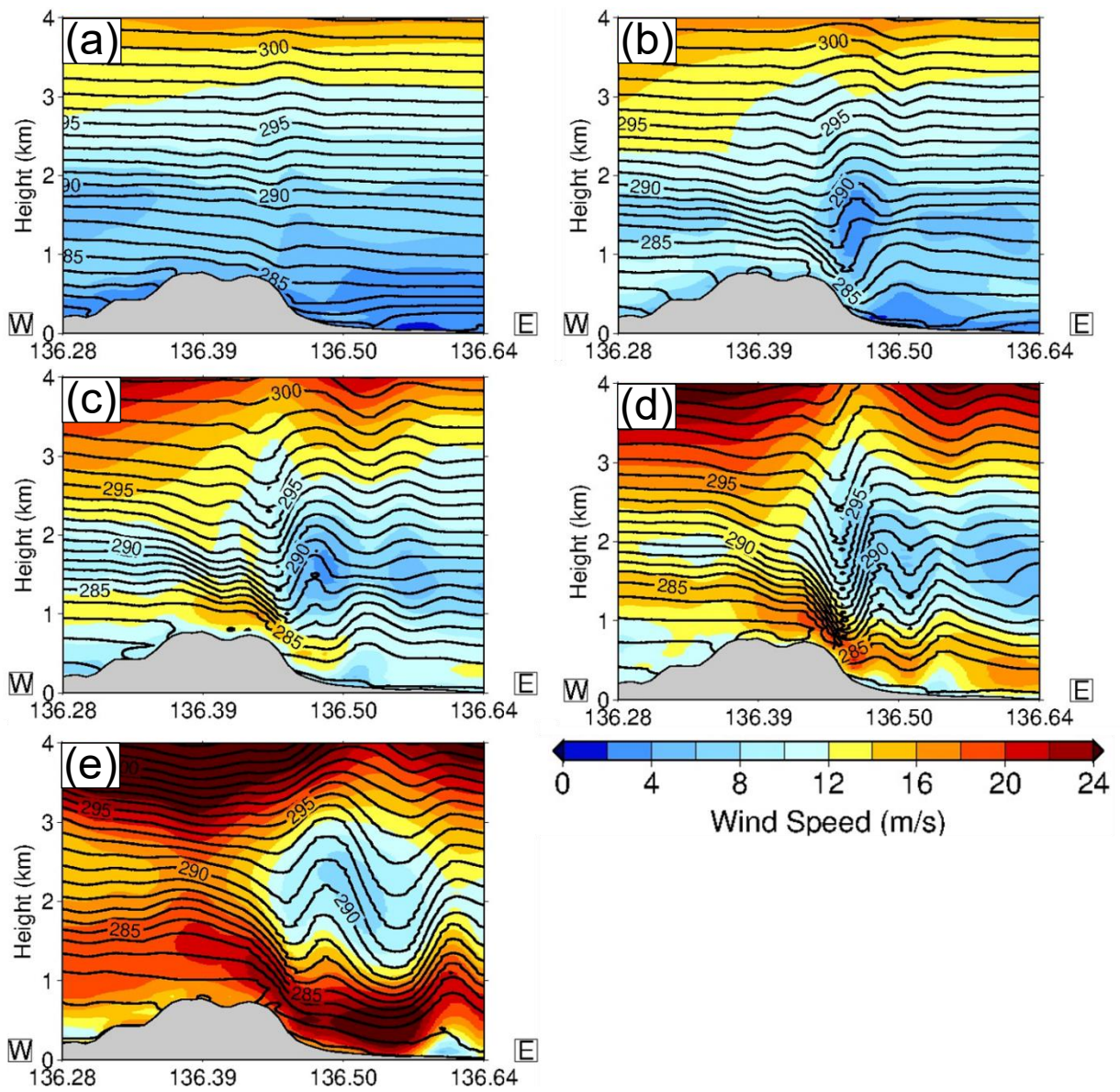
567 Fig. 7. Surface weather chart on March 5, 2014. (a) 0900JST. (b) 2100JST.



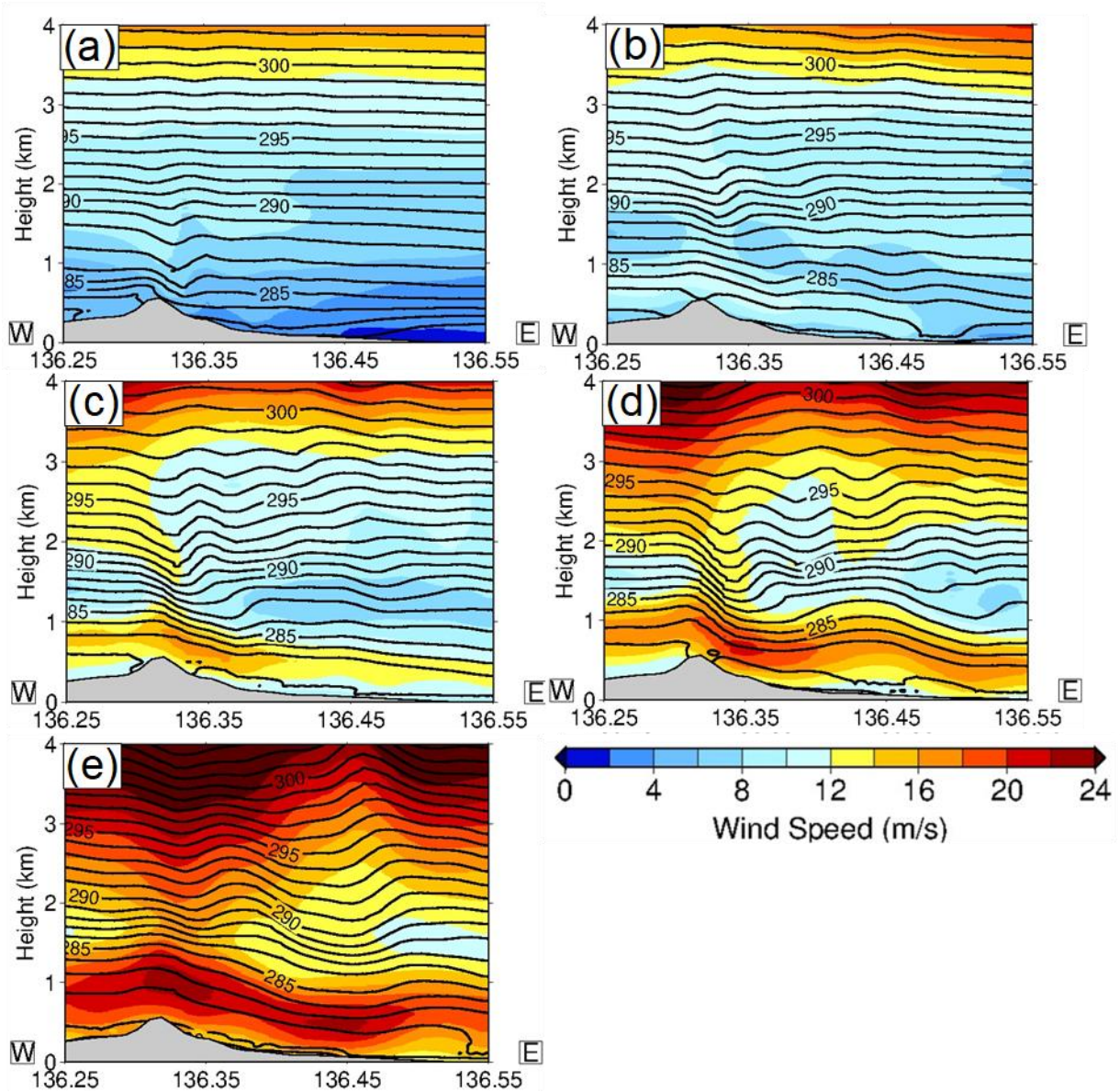
568 Fig. 8. Time series graphs of surface wind on March 5–6, 2014 JST. (a) Tsu (b) Komono.
 569 Upper and lower panels indicate wind speed and wind direction, respectively. Gray circle
 570 and line indicate results from observations. Black circles and line indicate results from the
 571 CTRL simulation.



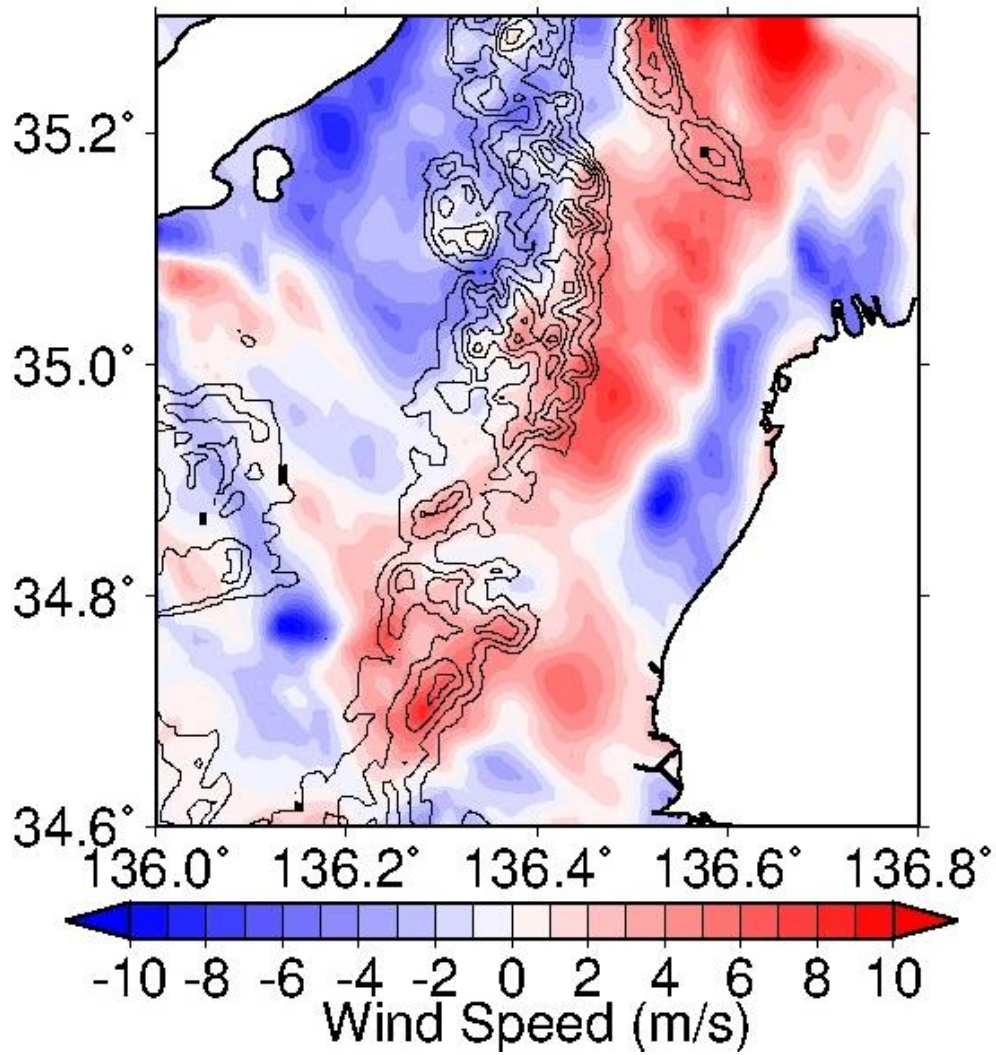
572 Fig. 9. Distribution of surface winds leeward of the Suzuka Mountains. (a) Results from
 573 observations at 1700 on March 5, 2014, JST. (b) Results from CTRL simulation at 1700 on
 574 March 5, 2014, JST.



575 Fig. 10. Vertical cross section of isentropes from CTRL simulation across the northern
 576 Suzuka Mountains (line A in Fig. 3) on March 5, 2014 (CTRL simulation). (a) 1200 JST. (b)
 577 1300 JST. (c) 1400 JST. (d) 1500 JST. (e) 1600 JST. Shade and contour indicate horizontal
 578 wind speed (m/s) and potential temperature (K), respectively.



579 Fig. 11. Vertical cross section of sentropes from CTRL simulation across the southern
 580 Suzuka Mountains (line B in Fig. 3) on March 5, 2014. (a) 1200JST. (b) 1300JST. (c)
 581 1400JST. (d) 1500JST. (e) 1600JST. Shade and contour indicate horizontal wind speed
 582 (m/s) and potential temperature (K), respectively.



583 Fig. 12. Impacts of mountains on the surface wind speed (cases CTRL - NoMt) at 1700 on
584 March 5, 2014, JST. Shade and contour indicate wind speed and elevation with 200m
585 contour interval.

586 Table 1. Surface observation data.

587

	Number of points	Period	Time interval
●AMeDAS	5	2012/1/1– 2016/12/31	10 min
□Atmospheric Environmental Regional Observation System	15		
▲ Observation point on the highways	4		

588

589 Table 2. Model configuration.

590

Model	WRF model, version 3.9.1
Grid spacing	1.0 km
Number of grid points	398 × 648 grid points
Number of vertical layers	50 vertical sigma levels
Boundary layer scheme	Yonsei University (YSU) PBL scheme
Simulation period (JST)	2014/03/05/ 0300–2014/03/07 0300
Initial/boundary condition	JMA-mesoscale analysis
Land use and terrain height	GSI digital national land information

591

592 Table 3. Breakdown of typical weather patterns during Suzuka-oroshi events.

593

	Number of Suzuka-oroshi events
"Kanto-Sanriku extratropical cyclone type" (Fig. 2a)	7
"Hokkaido-Okhotsk extratropical cyclone type" (Fig. 2b)	2
"Extratropical cyclone through Sea of Japan type" (Fig. 2c)	27
"High-pressure approaching type" (Fig. 2)	2
"Typhoon type" (Fig. 2e)	6
Other	1

594

595 Table 4. Presence of inversion layer and wind speed approaching the mountains during
 596 Suzuka-oroshi events.

597

		Presence of the inversion layer		
		Presence	Absence	Missing data
Wind speed approaching the mountains (m s ⁻¹)	0–6	13	0	0
	6–12	16	5	2
	>12	2	4	0